ACS OMEGA

http://pubs.acs.org/journal/acsodf

Article

Smart pH-Responsive Polyaniline-Coated Hollow Polymethylmethacrylate Microspheres: A Potential pH Neutralizer for Water Purification Systems

Dhiraj Dutta, Rama Dubey, Jyoti Prasad Borah, and Amrit Puzari*

Cite This: *ACS Omega* 2021, 6, 10095−10105

Read Online

ACCESS | Metrics & More | Article Recommendations

ABSTRACT: Smart materials with potential pH controllability are gaining widespread concern due to their versatile applicability in water purification systems. A study presented here demonstrates a successful synthesis of smart pH-responsive polyaniline (PANI)-coated hollow polymethylmethacrylate microspheres (PHPMs) using a combination of solvent evaporation and in situ coating techniques. The material was characterized by using conventional techniques. Images recorded by an optical microscope displayed clear evidence in support of the coating, which was further supported by the SEM images. Surface roughness due to the coating was distinct in the SEM images. The PANI coating has enabled the microsphere to effectively neutralize the pH of water in water purification systems, which is very important in tackling the excessive acidic or basic problem of water resources. This study introduces a simple, facile, and cost-effective synthetic route to develop polyaniline-coated hollow polymethylmethacrylate microspheres with high performance as a pH-responsive material for water purification. The low density of the material and relatively large surface area compared to conventionally used chemicals further enhance the application prospect of the material.

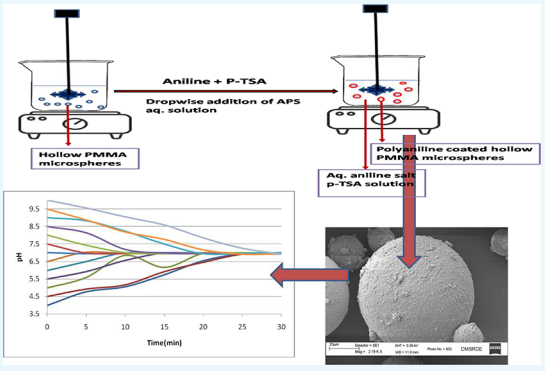

1. INTRODUCTION

Although water is abundantly present on the earth, the percentage of potable water[1] is only 2.5% and a major portion[2,3] of this is locked in polar ice caps. Again due to the alarming growth of population, water consumption has increased drastically,[4,5] leading to severe water scarcity worldwide. In addition, available water sources are largely contaminated with toxic effluents due to the increase in urbanization and rapid growth of industrialization,[6,7] eventually causing a major threat to human health and the environment.[8−13] Recent surveys have reported that drinking water in various countries does not meet WHO standards.[13−16]

Therefore, much scientific research has been focused on the development of robust new methods of water purification at lower cost[17−20] and using less energy while, at the same time, minimizing the use of chemicals that harm the environment. Among other parameters, pH is a key factor in the treatment of contaminated water[21] and it influences the efficiency and performance of the process.[22,23] Even in many cases, pH adjustment is a must for the removal of specific contaminants.[24] After contaminant removal at the required pH, the effluent water pH has to be adjusted[25] to neutral before delivery for human consumption to ensure health safety.[26] Drinking water with a very high or very low level of pH is potentially harmful to human consumption.[22,27] Drinking water with a pH less than 2.5 can cause irreversible damage to the epithelium.[28] The development of cost-effective simple materials for pH adjustment or neutralization is thus an urgent need.

Polymeric adsorbents modified by surface coating with different types of active/functional materials have recently been gaining importance for the development of such materials for water purification.[29−31] Functionalized hollow micro- and nanospheres are finding applications in various fields such as catalysis, water purification, drug delivery, electronic materials, and so on.[32,33] Several physical and chemical methods have been developed for preparing functional hollow polymeric particles and polymethylmethacrylate (PMMA) is one such potential polymeric candidate.[34−37] Usually, the inert nature of most of the polymers restricts their application in various fields. Therefore, surface modification of polymers must be carried out to improve their physicochemical properties. Specific moieties can be grafted or coated on the polymer

Received: January 6, 2021
Accepted: March 11, 2021
Published: March 19, 2021

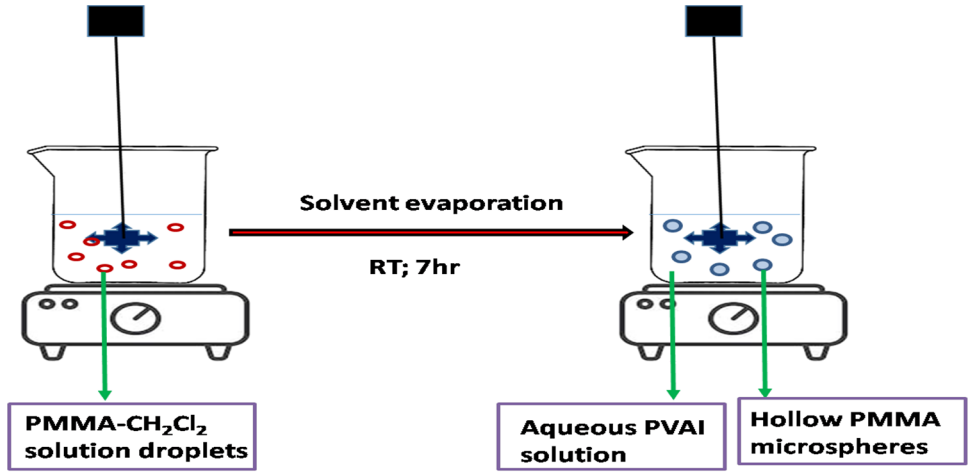

(a)

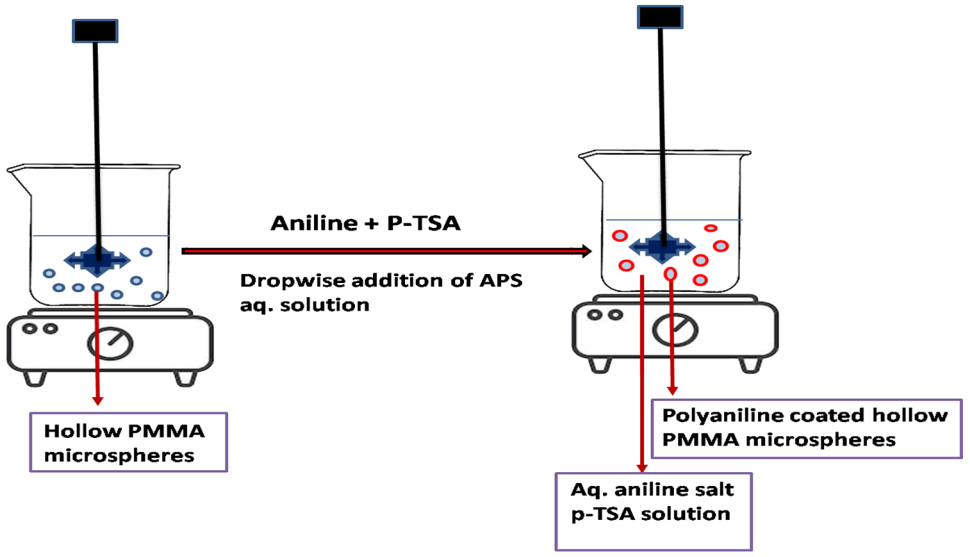

(b)

Figure 1. Schematic diagram for preparation of (a) PMMA and (b) PANI-coated PMMA microspheres.

surface to improve polymer performances.[38,39] Surface functionalization of PMMA with metal oxides, nanoparticles, or different polymers leads to the development of smart materials for important industrial applications.[40,41] Several surface functionalization methods are available in the literature. Adequate design and synthesis of functional hollow microspheres can lead to the development of materials that can respond intelligently to changing temperature,[42] electric fields[43] and magnetic fields,[44] pH and ionic strength,[45,46] and so on. Apart from these, the monodispersity of the hollow microspheres is also important in improving their material performances. Therefore, the design and synthesis of functionalized hollow microspheres with stimuli-responsive properties still warrant further exploration.

Polyaniline (PANI), one of the oldest known conducting polymers, is still being looked upon as a promising material for the development of new materials due to their prominent insulator-to-conductor transition through protonation. Polyaniline also attracts the interest of the scientific community due to its ease of synthesis, cost-effective nature, and good environmental, thermal, and chemical stability.[47−52] Therefore, PANI has also been used in interface science to develop smart materials with super-wetting surfaces and such pH-responsive polyaniline coating has been successfully used for effective separation of a complex oil−water mixture.[53,54] Hollow polymethylmethacrylate microspheres, due to their inherent physicochemical properties, offer themselves as a prospective material for surface functionalization to develop intelligent materials for scientific and technological applications.[55−57]

This article discusses the synthesis of PANI-coated hollow polymethylmethacrylate microspheres (PHPMs) as a pH-responsive material for the treatment of contaminated water. The PANI coating has enabled the material to respond intelligently for adjustment of pH during treatment of contaminated water. The advantages such as cost-effectiveness,

https://doi.org/10.1021/acsomega.1c00083
ACS Omega 2021, 6, 10095−10105

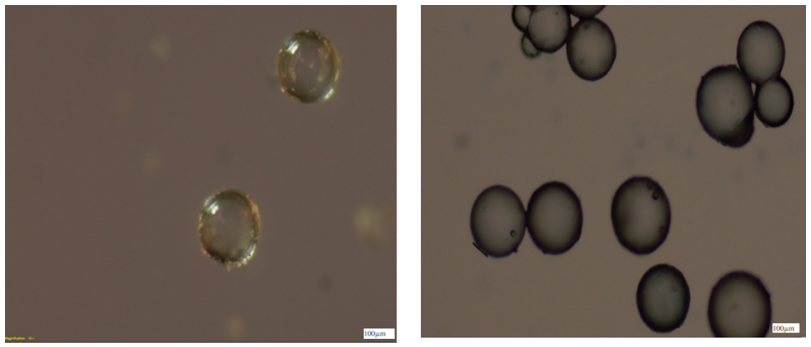

(a) (b)

Figure 2. Optical microscopy images of (a) PMMA microspheres and (b) PANI-coated PMMA microspheres.

the possibility of reuse, and the nonconsumable and non-chemical nature of the process are also highlighted.

2. MATERIALS AND METHODS

2.1. Materials. Polymethylmethacrylate (PMMA) [Sigma-Aldrich; MW (avg.): 120,000; 98%; viscosity: 0.20 dL/g(lit.)], dichloromethane (Merck; 99.5%; M = 84.93 g/mol), polyvinyl alcohol [Central Drug House, Delhi; MW (avg.): 125,000; 99.25%; viscosity: 35−50 cP at 4% cold aqueous solution], p-toluenesulfonic acid monohydrate (Merck; ACS reagent, ≥98.5%), ammonium persulfate (Merck; ACS reagent, ≥98.0%), hydrochloric acid (Merck; fuming 37%, for analysis EMSURE ACS, ISO, Reag.), sodium hydroxide (Merck; pellets EMPLURA), ethyl alcohol (AR 99.9%; Jiangsu Huaxi International China), and ammonium hydroxide solution (28% NH_3 in H_2O, ≥99.99% trace metal basis; Sigma-Aldrich) were used as received. All solutions were prepared using double-distilled water. All other reagents used were of analytical grade and were obtained from Merck, India.

2.2. Preparation of PMMA Microspheres. Hollow PMMA microspheres (HPMs) were prepared by using the solvent evaporation technique.[37] In the first step, a solution was prepared by dissolving PMMA (5−6%, w/v) in dichloromethane through continuous stirring in a magnetic stirrer. The solution was added dropwise to a stirring aqueous medium. The aqueous medium comprises 0.5% (w/v) polyvinyl alcohol, which acts as a stabilizer. The stirring was maintained at 550 rpm with a propeller-type mechanical stirrer. Hollow PMMA microspheres (HPMs) were formed by slow evaporation of dichloromethane at room temperature. At the end of the reaction, HPMs are obtained after washing with water and drying at 70 °C. The bulk density of the HPMs was calculated as 0.69 g/cc.

2.3. Preparation of Polyaniline-Coated HPMs. Polyaniline (PANI)-coated HPMs were prepared by using a process similar to the already reported process for polyaniline coating on an HPM surface.[37,58] PMMA microspheres obtained above were suspended in the polymerizing mixture used for polyaniline synthesis for coating. The Schematic diagram for preparation of (a) PMMA and (b) PANI-coated PMMA microspheresis shown in Figure 1.

Aniline (10 mmol) and a doping agent (p-TSA) (10 mmol) were dissolved in distilled water and the volume was made up to 50 mL with distilled water. Four grams of microspheres was suspended in the polymerization mixture followed by dropwise addition of 12.5 mL of 1 M aqueous ammonium peroxydisulfate solution with constant stirring. A magnetic stirring of the polymerization mixture was maintained approximately at 200 rpm at room temperature. The polymerization mixture gradually turned darkish blue and finally a green color, indicating the completion of the polymerization. The reaction mixture was then allowed to stand overnight.

The sediment of PANI-coated hollow PMMA microspheres (PHPMs) was collected and redispersed in a 0.2 M aqueous solution of doping agent (p-TSA). The coated microspheres were collected on a filter and washed with excess water and several aliquots of methanol until the runoff becomes clear. Finally, the product was dried under vacuum at 50 °C. The bulk density of PHPMs was calculated as 1.27 g/cc.

2.4. pH Regulatory Study. For the pH regulatory study, 10 mL of solution of different pH values was taken separately in a 50 mL beaker and 1 g of PHPMs was added to each. Before starting the experiment, the pH was adjusted with dilute HCL and 0.1 N NaOH without buffer. Once PHPMs were added, the addition of any other material was avoided. The temperature was maintained at 25 °C by operating a common air conditioner. The change in pH was recorded with the pH meter. The pH meter was calibrated after each set of testing at a particular pH. The same study was carried out using a UV−Vis spectrophotometer at 600 nm. The absolute absorbance was recorded as received after taking water as a reference.

2.5. Characterization of Materials. Materials characterization was performed by using an optical microscope with a Leica DMLM/P (Leica Microsystems AG, Switzerland) at 50× magnification, scanning electron microscope (Carl ZEISS, EVO50), transmission electron microscope (JEOL 200 kV, model no. JEE2100), FTIR spectrophotometer (Bruker Alpha model with KBr), thermogravimetric analyzer (TA Instrument USA, models 2950 and 2910), UV−Visible spectrophotometer (double-beam spectrophotometer from Analytik Jena model SPECORD 205), and atomic force microscope (model Nanonics Multiview 2000AFM with a fiber probe). The isoelectric measurement was carried out by using a Horiba SZ-100 with autotitrator ζ-potential measurement at different pH values. Particle size analysis was carried out using a submicron particle sizer NICOMP 380 (Particle Sizing Systems, California, USA) with an Accusizer 780A Autodiluter. Electrical conductivity was measured by using a multi-parameter model EuTech CD 650.

3. RESULTS AND DISCUSSION

3.1. Characterization of HPMs and PHPMs by Optical Microscopy. The optical micrographs of uncoated and PANI-

https://doi.org/10.1021/acsomega.1c00083
ACS Omega 2021, 6, 10095−10105

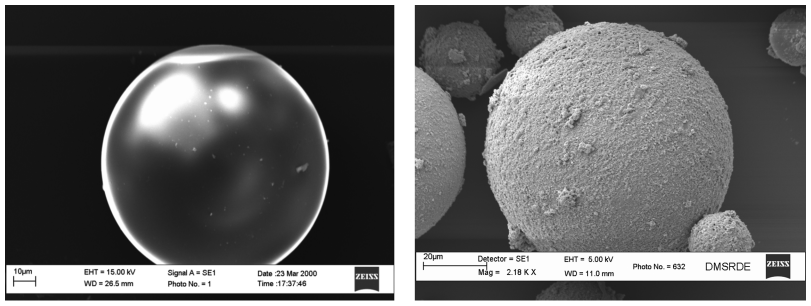

(a) (b)

Figure 3. SEM images of (a) a PMMA microsphere and (b) PANI-coated PMMA microspheres.

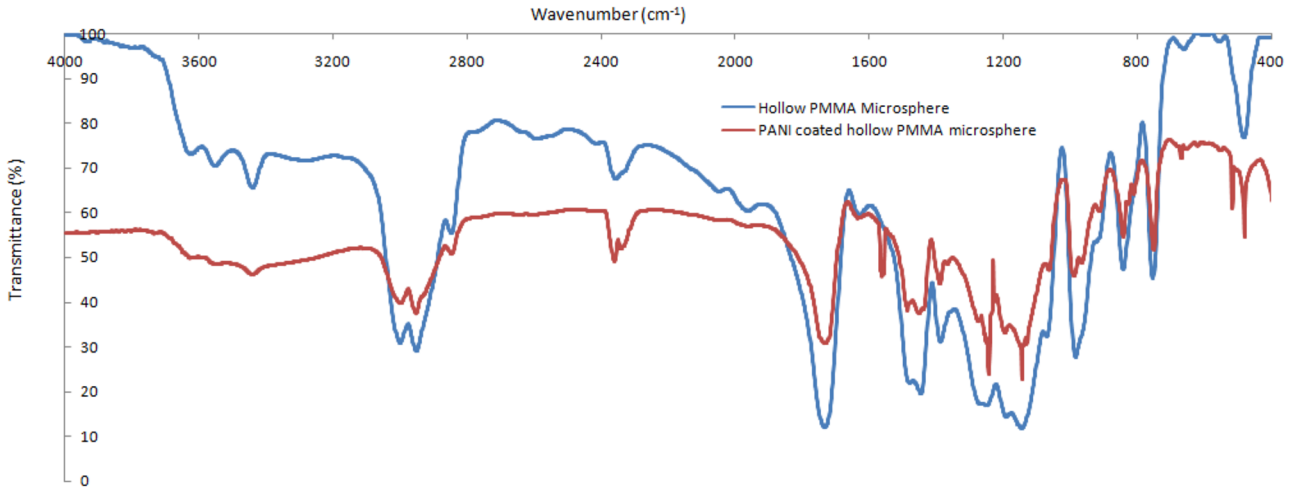

Figure 4. FTIR spectra of hollow PMMA and PANI-coated PMMA microspheres.

coated PMMA microspheres are shown in Figure 2. The diameter of PMMA microspheres was between 20 and 80 μm. The bulk density of PMMA microspheres was measured to be 0.69 g/cc. A thick dense PANI coating was observed on the surface of PMMA microspheres. Under the optical microscope, the uncoated PMMA microspheres appeared as small transparent hollow spheres, whereas coated PMMA microspheres (Figure 2) appeared as dark green spheres. The dark green color of the PANI-coated HPM is due to the deposition of green color-conducting PANI salt on the surface of microspheres. The coating is not smooth due to the adhesion of PANI in the form of a precipitate, which is formed in the reaction medium.

Clear visualization of PANI coating on the surface of the PMMA microsphere was noted in the optical micrographs. The micrographs indicate the whole coverage of the PMMA microsphere with PANI. A low concentration of reactants was maintained to avoid the macroscopic precipitation of PANI over the surface of the PMMA microsphere. Further exposure of microsphere surface to the excess PANI precipitate resulted in the thick deposition of agglomerated PANI particles. It has been reported that once polymerization of polyaniline is carried out in the presence of foreign particles, surface polymerization precedes the precipitation polymerization in the bulk.[59] In this study, it is anticipated that polymerization occurs on the surfaces of microspheres. Moreover, the distinct sedimentation rate of the coated microspheres allowed the separation of the same from the PANI precipitate. It has been estimated that the PANI coating on PMMA microspheres was approximately 18 wt % when coated with PANI-PTSA.

3.2. Characterization of HPMs and PHPMs by Scanning Electron Microscopy (SEM). The morphologies and surface texture of PMMA microspheres before and after PANI coating were observed by SEM as shown in Figure 3. Figure 3a shows that the PMMA microsphere possesses a perfectly spherical shape with a smooth surface before coating. The magnified image of the PANI-coated PMMA microspheres is shown in Figure 3b, which reveals that the microspheres have a diameter in the range of 20−80 μm. On the other hand, from Figure 3b, it is also evident that coating of PANI over the PMMA microspheres results in surface roughness and the PANI coating has covered a sizeable portion of the PMMA surface. Increased surface roughness also increases the hydrophobicity of the PANI-coated PMMA microspheres. Parida et al.[60] have suggested that the perfect spherical shape retained in SEM indicates that the microspheres must be able to withstand vacuum and the electron beam that can damage the polymer. The mean size obtained by SEM was comparable with results obtained by the dynamic light scattering study of size distribution.

3.3. Characterization of HPMs and PHPMs by FTIR. FTIR measurements were employed to determine changes in the chemical composition of PMMA microspheres before and after PANI modification and the same is represented in Figure 4. Specific absorption bands revealing the presence of various functional groups are observed. Specific bands from 1150 to 1250 cm^{-1} can be attributed to the C−O−C stretching

https://doi.org/10.1021/acsomega.1c00083
ACS Omega 2021, 6, 10095−10105

vibration, and the two bands at 1388 and 750 cm^{-1} can be attributed to the α-methyl group vibrations.

The band at 987 cm^{-1} is the characteristic absorption vibration of PMMA, together with the bands at 1062 and 845 cm^{-1}. The band at 1740 cm^{-1} shows the presence of the acrylate carboxyl group. The band at 1440 cm^{-1} can be attributed to the bending vibration of the C−H bonds of the $-CH_3$ group. The two bands at 2998 and 2942 cm^{-1} can be assigned to the C−H bond stretching vibrations of the $-CH_3$ and $-CH_2-$ groups, respectively. Furthermore, there are two weak absorption bands at 3437 and 1648 cm^{-1}, which can be attributed to the −OH group stretching and bending vibrations, respectively, of physisorbed moisture.

In addition to the above-mentioned absorption bands on PMMA, characteristic peaks of PANI are also observed, including broad peaks over the range of 3016.67−3417.86 cm^{-1}, corresponding to N−H stretching vibrations of secondary amine. The sharp peak at 1560.41 cm^{-1} can be attributed to C═C stretching of the quinoid ring (N═Q═N) and the peaks at 1413.82 and 1475.54 cm^{-1} are characteristic peaks of C═C stretching vibration of the benzenoid ring (N−B−N). Similarly, FTIR absorption at 1244.09 and 1298.09 cm^{-1} corresponds to C−N stretching of a secondary aromatic ring, the one at 1130.29 cm^{-1} indicates the presence of aromatic C−H in-plane bending vibrations, and the ones at 611.43, 719.45, and 804.32 cm^{-1} are attributed to aromatic C−H out-of-plane bending vibrations. These peak positions match well with those reported in the literature.[61,62] Ajeel and Kareem[63] have explained the above peak in detail for the PMMA and graphene interaction.

3.4. Characterization of HPMs and PHPMs by UV−Vis Spectroscopy. Polyaniline generally switches between two forms reversibly, i.e., conducting emeraldine salt and nonconducting emeraldine base forms depending on its environment. Under low pH or acidic conditions, it exists in the form of conducting salt. In the presence of a base or high pH, it gets converted from its conducting form into the nonconducting form. The conducting form is green in color, whereas the nonconducting form displays a blue color (Figure 5).

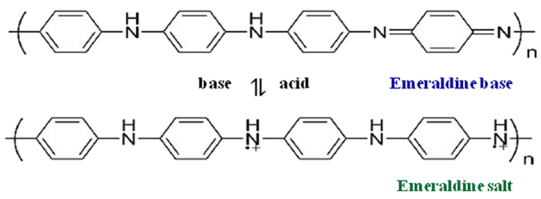

Figure 5. Emeraldine base and emeraldine salt forms of PANI.

The UV−Vis absorption spectra of the PMMA microspheres before and after PANI modification were recorded in the 300−1100 nm region and the same is displayed in Figure 6. The spectra for undoped PANI (emeraldine base) show two characteristic absorption bands at around 330 and 620 nm corresponding to $\pi \rightarrow \pi^*$ transition of benzenoid and quinoid rings of PANI, respectively.[64]

The decrease in the absorption band at about 620 nm in the case of doped PANI indicates that the amine nitrogen atoms of the quinoid rings are converted to benzenoid rings due to protonation by dopants. Upon doping, the quinoid transition disappears and two new absorbances occur. These new absorbances point at 420 and 800 nm.

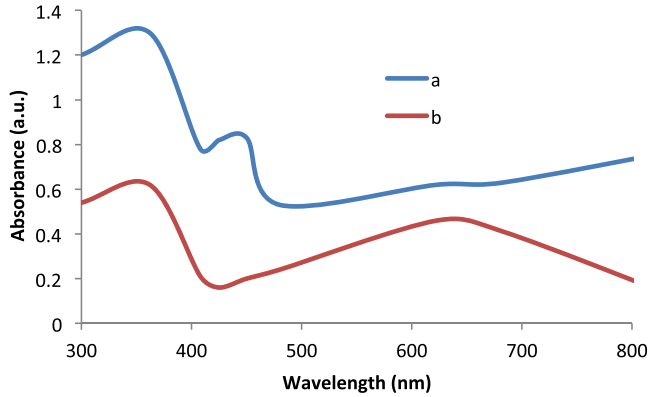

Figure 6. UV−Vis absorption spectra of (a) PMMA microspheres and (b) PANI-coated PMMA microspheres.

3.5. Characterization of HPMs and PHPMs by AFM. The atomic force microscopy (AFM) images recorded for HPMs and PHPMs are represented in Figure 7, and the images were recorded under noncontact mode. A scan of 10 μm in both directions is performed on the surface of the PHPM. The total path length of contact mode touch is 0.55 μm at a Pt angle of 0.14°. A well-spread dotted surface is observed during the scanning of the curved surface. The curved spherical surface of the microsphere is one of the difficult surfaces to scan by AFM. Therefore, the noncontact mode is selected for scanning because contact mode may damage the tip of the atomic force microscope. The scanning topograph shows a uniform layered deposition, which is in contrast to the uneven rough surface of the microsphere observed in the optical and SEM micrographs. This further can be imagined as the deposition of a single layer as a single layer is a very much uniform. Multiple-layer deposition, which does not cover the entire surface, leads to an uneven surface.

The same deposition phenomena were studied by Mishima et al.[65] with crosslinked rubber-coated microsphere films. Once a single layer of the meniscus formed, a downward force acted on the spheres to embed them into the PANI film. Deposition eventually decreases when the angle between the tangential line of the sphere and the PANI surface became equal to the equilibrium. Interestingly, the deposition behavior was nearly identical for spheres with a plain film.

3.6. Characterization of HPMs and PHPMs by TEM. TEM measurements are carried out by using a small quantity of sample along with ethanol, which was taken in a test tube and sonicated for 20 min in a sonication bath. After sonication, one or two drops of the sample solution were deposited on a carbon-coated copper grid. The grid was rested on a Whatman filter paper for the absorption of excess solvent and dried for 5−10 min to enable the evaporation of any remaining solvent. After complete drying, the sample-coated grid was used for TEM measurements. TEM images of HPMs and PHPMs are shown in Figure 8a,b, respectively. It has been observed from the two micrographs that the PANI coating is well spread over the surface of the HPM and PHPM. However, some edges of uneven coating are also observed, which are hard to avoid especially for small particles. In general, a coating of PANI on the PMMA surface is often critical to obtain. The uneven edges of the rough surface will also influence the aspect ratio (as the average diameter will change), which in turn may influence the surface texture of the polymeric microspheres. It is also possible that the coating of PANI might have overlapped along

https://doi.org/10.1021/acsomega.1c00083
ACS Omega 2021, 6, 10095−10105

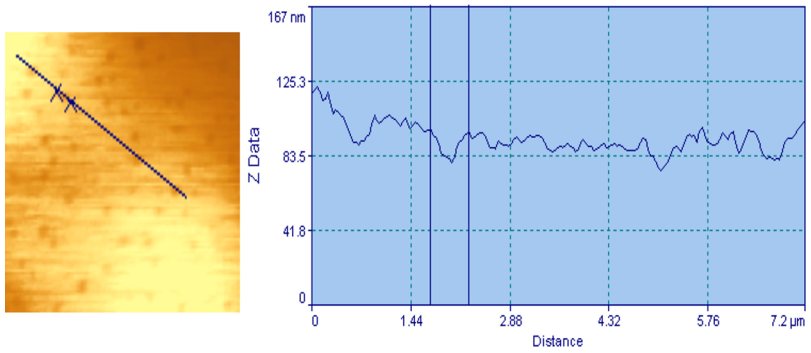

Figure 7. AFM topograph of PANI-coated PMMA microspheres.

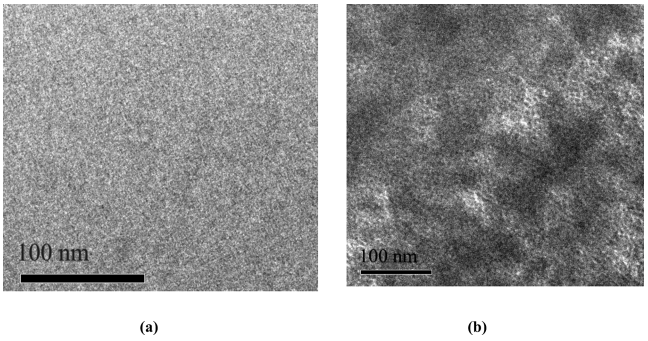

Figure 8. TEM images of (a) PMMA microspheres and (b) PANI-coated PMMA microspheres.

the depth direction of the specimen (i.e., *Z*-direction) because of which poor resolution along this direction in the TEM images is observed. The surface texture of the HPM and PHPM is completely different. The study confirms a random coating of PANI over the PMMA surface. The uneven surface confirms that the interaction between the surfaces is rather physical than chemical. This has further been confirmed by other subsequent studies.

3.7. Characterization of PHPMs for Particle Size Analysis. Figure 9 shows the size distribution of PHPMs.

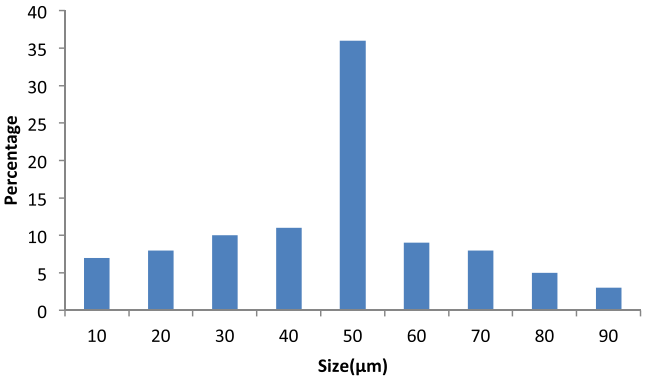

Figure 9. Particle size analysis of PANI-coated PMMA microspheres.

From the microscopic study, it is confirmed that the PHPM is mainly in the micrometer range ranging from 10 to 90 μm. The size distribution study is one of the important parameters in any spherical material. Even though the size distribution can be manipulated by separation techniques like sieving through the mesh, vibrational separation, centrifugation, etc., the basic size distribution contributes to a great extent to the bulk property of the material. Here, the observation is that a maximum of about 36% of the material is in about 50 μm range. It is also observed that about 7% of the material is in about 10 μm range, which increases gradually to 8% for 20 μm, 10% for 30 μm, 11% for 40 μm, and 36% for 50 μm. But it again gets drastically reduced to 9% for 60 μm, 8% for 70 μm, 5% for 80 μm, and 3% for 90 μm. The rest of the material is negligible from other size ranges. The materials are used with the same size distribution in all other studies without any size modification. The size distribution study goes hand in hand with micrographs of SEM and optical microscopy studies.

3.8. Conductivity Measurement of PHPMs against Variation of pH. The electrical conductivity (EC) of PHPMs at various pH values is plotted in Figure 10. The neat

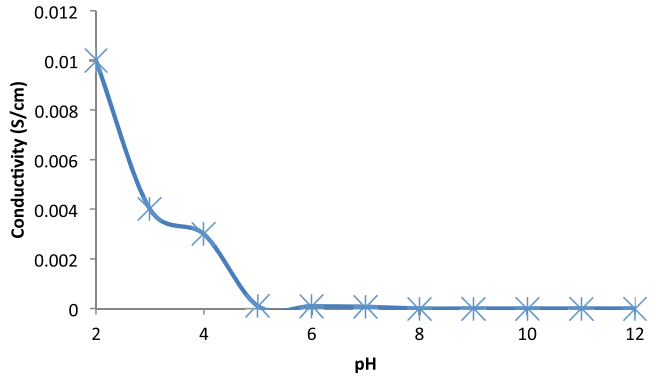

Figure 10. Conductivity measurement of PHPMs against variation of pH.

polyaniline film coating on the surface of PMMA microspheres showed an EC of 1.72 S cm^{-1}. As displayed in Figure 10, the EC of the PHPM surface decreases with an increase in the pH of the solution. The decrease in conductivity was drastic until pH 5 and, beyond that point, the conductivity decreases slowly between pH 5 and pH 12. Since the conductivity at pH 7 was measured to be 0.00007 S cm^{-1}, hence, polyaniline can be considered as conductive (conductive plastic ranges up to 10^{-6} S cm^{-1}).[66] From pH 2.0, the conductivity starts decreasing by several folds in comparison to the polyaniline film, which may be due to deprotonation of PANI, because once the conductive form of PANI, i.e., the emeraldine salt, is formed, the addition of either a base or an acid leads to deprotonation or protonation of the base (−NH−) sites in PANI, which causes switching of PANI between different oxidation states.[67] It has been well established that the overall conductivity of polyaniline is due to interchain charge transport,[68] and its

https://doi.org/10.1021/acsomega.1c00083
ACS Omega 2021, 6, 10095−10105

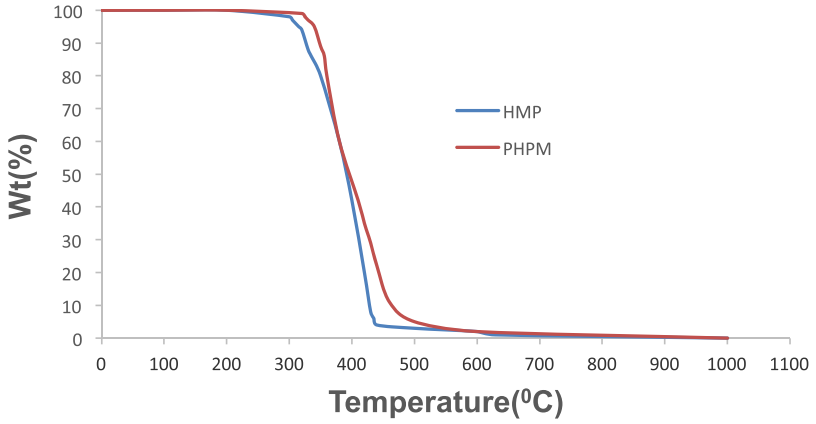

Figure 11. TGA of HPMs and PHPMs.

Table 1. Variation of ζ-Potential with Increasing pH

pH values	2	3	4	4.4	5	6	7	8	9	10	11	12
ζ-potential (mV)	+7	+4	+2	0	−1	−6	−14	−42	−52	−65	−71	−72.97

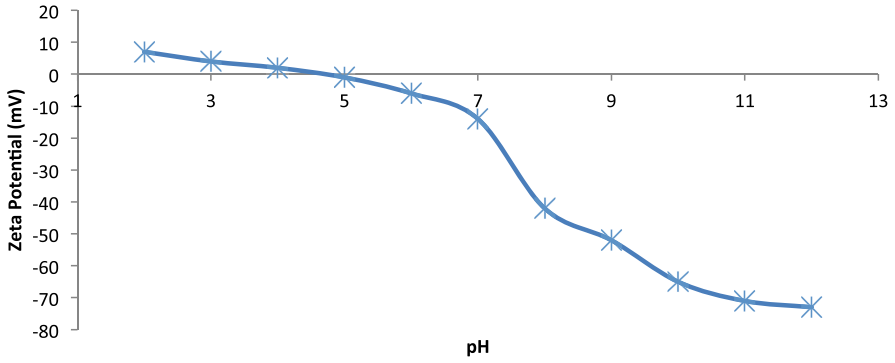

Figure 12. ζ-Potential study of the PHPM at different pH values to evaluate the isoelectric point.

mechanism depends on several factors, among which protonation (doping level) is one. The relationship between charge and doping has been well explained by MacDiarmid and Huang as the protonation/deprotonation of PANI, which results in an increase or decrease in the amount of charge on the polymer backbone, leading to increased or decreased conductivity.[69,70] The relationship between charge and doping has been explained in a study reported in the literature,[71] which mentioned that during the deprotonation of PANI, the interaction between a polar molecule and PANI decreases, which results in redistribution of charge and hence reduced electrical conductivity. Thus, based on the above discussions, it can be inferred that on the addition of NaOH to the protonated PHPM dispersion, the deprotonation of PANI starts. The initial deprotonation results in redistribution of charge because active sites for interaction between polar molecules and PANI are still present with changing pH but in reduced quantity. Therefore, at pH $\leq$ 5, there is a drastic reduction in EC of the materials, which implies a significant reduction in polymer backbone active sites. But, at pH > 5, there is a gradual fall in the EC of the PHPM dispersion, suggesting that all active sites of the polymer backbone have been removed. This suggests that polar molecules do not interact with PANI of the PHPM, resulting in the deprotonation of PANI. The EC and ζ-potential study results are complementary to each other.

3.9. Characterization of HPMs and PHPMs for TGA. The results of the thermogravimetric analysis (TGA) of HPMs and PHPMs are displayed in Figure 11. The analysis was performed in the temperature range from room temperature to 600 °C, with the standard protocol of the instrument manufacturer. The sample HPM and PHPM show a similar trend with extreme stability until 220 °C, after which it shows drastic and gradual degradation until about 408 °C. Both the polymeric entities exhibited clear distinction in their degradation pattern as reflected in Figure 11. The HPM gets the characteristics of two-stage degradation, which is somewhat suppressed in the PHPM due to the polyaniline percentage of the PHPM. The second stage of HPM decomposition is due to the decomposition of the unsaturated chain ends of PMMA. It is also clear from the study that this is not a blend of two polymers. On the contrary, it is a physically deposited coating on the surface of one polymer, which is PMMA by another polymer that is polyaniline. From the thermogravimetric analysis, the percentage of polyaniline coating is evaluated to be 18% (w/w).

3.10. ζ-Potential Study to Evaluate the Isoelectric Point of the PHPM. To investigate the variation of surface charge of the PHPM with pH, the ζ-potential measurements of PHPM aqueous suspensions were performed at different pH values ranging from 2 to 12 by using a zeta potential analyzer (Malvern, U.K.). The changes in the ζ-potential values as a

https://doi.org/10.1021/acsomega.1c00083
ACS Omega 2021, 6, 10095−10105

Table 2. Variation of Time to Achieve the Neutral Point from Different pH Values

time (min)	pH 4	pH 4.5	pH 5	pH 5.5	pH 6	pH 6.5	pH 7	pH 7.5	pH 8	pH 8.5	pH 9	pH 9.5	pH 10
0	4	4.5	5	5.5	6	6.5	7.00	7.5	8	8.5	9	9.5	10
5	4.76	4.93	5.60	5.93	6.49	7.03	6.95	6.99	7.42	8.14	8.83	8.88	9.55
10	5.05	5.16	6.86	6.56	7.00	6.96	6.96	6.96	7.01	7.19	8.24	8.19	9.04
15	5.75	5.93	6.16	6.98	6.96	6.99	7.00	6.97	6.95	6.99	7.49	7.76	8.58
20	6.54	6.46	6.96	6.95	6.95	7.00	6.97	6.95	6.96	6.96	6.95	7.17	7.85
25	6.95	6.92	6.96	6.95	6.97	6.95	6.96	6.98	7.00	6.95	6.97	6.92	7.26
30	6.93	6.95	6.95	6.98	6.98	6.96	6.99	6.96	6.99	6.96	7.00	6.95	6.91

Table 3. Variation of Dose of PANI-Modified PMMA to Achieve the Neutral Point from Different pH Values

dose (mg)	pH 4	pH 4.5	pH 5	pH 5.5	pH 6	pH 6.5	pH 7	pH 7.5	pH 8	pH 8.5	pH 9	pH 9.5	pH 10
0	4	4.5	5	5.5	6	6.5	7.0	7.5	8	8.5	9	9.5	10
5	4.8	4.97	5.65	5.98	6.55	7.09	7.01	7.05	7.48	8.21	8.91	8.96	9.63
10	5.1	5.21	6.92	6.62	7.06	7.02	7.02	7.02	7.07	7.25	8.31	8.26	9.12
15	5.8	5.98	6.21	7.04	7.02	7.05	7.06	7.03	7.01	7.05	7.56	7.83	8.65
20	6.6	6.52	7.02	7.01	7.01	7.06	7.03	7.01	7.02	7.02	7.01	7.23	7.92
25	7.01	6.98	7.02	7.01	7.03	7.01	7.02	7.04	7.06	7.01	7.03	6.98	7.32
30	6.99	7.01	7.01	7.04	7.04	7.02	7.05	7.02	7.05	7.02	7.06	7.01	6.97

function of suspension medium pH are depicted in Table 1. It is observed from the table that ζ-potential values for the PHPM decreased with an increasing suspension of pH. At low pH values of about 2, 3, and 4, the ζ-potential values were +7, +4, and +2 mV, respectively. The positive ζ-potential values at low pH indicate the protonation of polyaniline, resulting in positive charges on the surface as has already been shown for the doping of pure polyaniline dispersions.[72] As the pH was increased, the surface charge density started decreasing due to the dedoping of polyaniline with increasing pH. The isoelectric point of PHPM suspension was measured to be around pH 4.4, which is the pH value when the ζ-potential becomes zero (Figure 12). On further increasing the pH, the ζ-potential values decreased slowly until pH 5 and drastically beyond pH 5 until pH 12. At pH 5, the ζ-potential value was −1 mV, at pH 6, the ζ-potential value was −6 mV, at pH 7, the ζ-potential value was −14 mV, at pH 8, the ζ-potential value was −42 mV, at pH 9, the ζ-potential value was −52 mV, at pH 10, the ζ-potential value was −65 mV, at pH 11, the ζ-potential value was −71 mV, and at pH 12, the ζ-potential value was −72.97 mV. From the results, it can be inferred that the positive charge density on the surface of the PHPM decreased significantly with an increase in pH of the medium due to the deprotonation of amine groups on PANI. The charge density in the tested pH range changed from +7 to −72.97 mV.

3.11. Characterization of PHPMs for the pH Regulation Study. PANI-modified PMMA, i.e., the PHPM, is in semiconducting form. So, in water, the OH^- ion will be consumed by the conducting polyaniline, producing a blue color and resulting in a decrease in the conductivity of polyaniline, and the H^+ ion will be consumed by the nonconducting polyaniline, giving a green color and resulting in an increase in the conductivity of polyaniline.

Polyaniline-coated PMMA microspheres are low-density forms of polyaniline where the same amount of polyaniline was coated or dispersed over the surface of a hollow structure. The result of the testing shows that polyaniline can neutralize both acidic and basic water. The test result is shown in Tables 2 and 3. The testing is carried out from pH 4 to 10 with a variation of time and doses for high and low pH with a maximum distance from the neutral point that is pH 7. It is observed that more time is taken for neutralization when the pH is at far extreme values, both on the upper and lower sides, whereas the reverse is true for the nearest points. For example, for the sample with pH 4, it takes about 25 min to achieve pH 7.0, while the time taken to achieve pH 7.0 by the sample with pH 6.5 is only 5 min. For the basic pH, for the solution with pH 10.0, it takes 30 min to reach the neutral point, while for the solution with pH 8.0, it takes 10 min to reach the neutral point. This is due to an abundance of H^+ or OH^- ions in the solution. The higher the number of ions, the more time it takes to entrap the ion into the polymeric chain by self-converting from nonconducting to conducting form and vice versa. The same experiment was repeated with the variation of doses of PANI-modified PMMA. For the evaluation purpose, the observation time was fixed at 5 min. The results show that the higher the dose or amount of polyaniline-coated PMMA, the less time it takes to achieve the neutral point. It also depends on the amount of corrections to a neutral point in the pH scale. For example, a solution at pH 4.0 takes 25 mg of material to reach near the neutral point within a time frame of 5 min. On the same front, a solution with pH 5.0 takes only 20 mg of material to achieve the same. But there is no proportionate relation because the solution with pH 4.5 takes 30 mg of PANI-modified PMMA to reach closer to the neutral point.

On the basic front, for the case with pH 10.0, it takes 30 mg of materials to reach the neutral point, while it takes only 10 mg for the case with pH 8.0. The solution with pH 9.0 takes about 20 mg of dose and the one with pH 9.5 takes 30 mg. This also confirms our assertion that there is no proportionate relation for the number of doses required for solutions with different pH values to achieve the neutral point. It varies concerning various parameters like the amount of ions present in a solution, the dose of the material, time required, and the possibility of random ions coming in contact with the material. The change is not proportional because the number of ions increases with the increase and decrease in pH and more and more ions will come in contact with the polymeric chain of the PANI-coated hollow PMMA microsphere. This leads to faster consumption of ions by the polymeric chain to get converted to conducting form for H^+ ions and nonconducting form for OH^- ions.

https://doi.org/10.1021/acsomega.1c00083
ACS Omega 2021, 6, 10095−10105

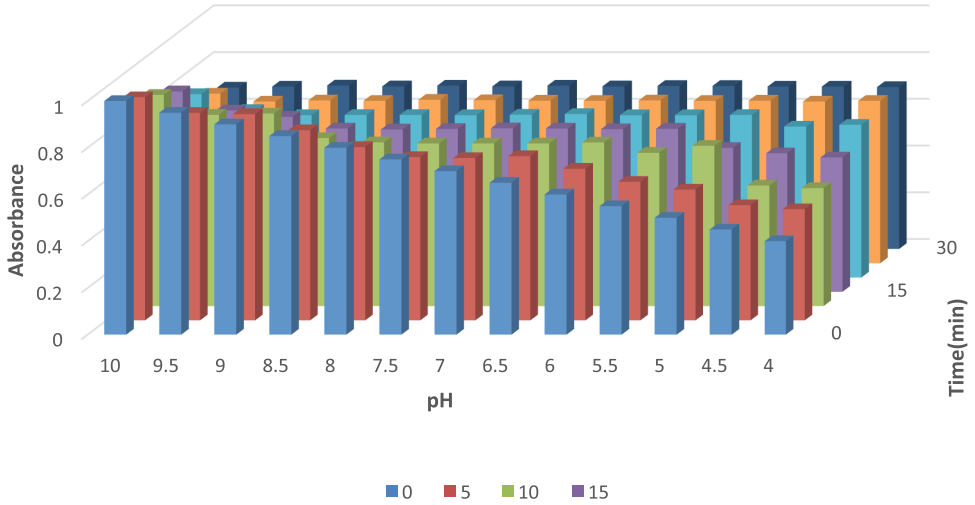

Figure 13. UV−Vis spectroscopy study of PHPMs at different pH values and time intervals.

As shown in Figure 13, a UV−Vis spectrophotometer was also used to study the absorption of PANI-coated PMMA microspheres at different pH values and times. The peak at 600 nm was taken as the reference peak. The findings indicate similar patterns to those in the study of dose variation and time variation. As stated in the literature,[69] with the change in conductivity, the absorbance at 600 nm also changes inversely.

It is observed that pH 4, which is the highest conductive point in this study, shows an absolute absorbance of 0.4, which increases up to 0.693 within 30 min of a time interval. This is in correlation to the fact that a similar time is required to neutralize a solution to pH 4 to pH 7. On the other hand, pH 4.5 shows an absolute absorbance of 0.45, pH 5 shows an absolute absorbance of 0.5, pH 5.5 shows an absolute absorbance of 0.55, pH 6 shows an absolute absorbance of 0.6, and pH 7 shows an absolute absorbance of 0.7. On a certain amount of exposure time, they have come down to the absolute absorbance value of 0.7, which resembles pH 7. On the basic front, pH 10, which is the highest basic value of this study, shows an absolute absorbance of 1, while pH 9.5 shows 0.95 absolute absorbance, pH 9 shows 0.9 absolute absorbance, pH 8.5 shows 0.85 absolute absorbance, pH 8 shows 0.8 absolute absorbance, and pH 7.5 shows 0.75 absolute absorbance. pH 7.5 takes a bare minimum time of fewer than 5 min to neutralize to pH 7, showing an absolute absorbance of 0.699, while pH 10 takes a maximum time of 20 min for the same. This study exactly resembles the study carried out by a pH meter and conductivity meter probe attached to the measuring system. This study further confirms the usability of the PHPM as a very versatile and accurate pH-regulating material.

4. CONCLUSIONS

In summary, polyaniline-coated hollow polymethylmethacrylate microspheres (PHPMs) were successfully synthesized using a combination of solvent evaporation and in situ coating technique. The material is capable of regulating the pH of the aqueous solution intelligently. In other words, a smart material that can be projected as a potential pH neutralizer for water purification was developed. The pH-regularizing efficiency depended on contact time, a dose of PANI-modified PMMA, and pH of the solution. Surface modification of PMMA microspheres induced by polyaniline coating enabled the material to respond smartly to the variation of pH of an aqueous solution. Experimental results showed that the PHPM can neutralize the pH for the solution with pH ranging from 4 to 10 and a contact time of 30 min was sufficient to achieve the neutralization. So, we can reasonably conclude that the material developed will have extensive commercial utility as it is capable of working as a viable alternative for the commercially available pH buffer and single-side regulators such as limestone or phosphoric acid for the decontamination of polluted water, which is largely used in any community-type water purification system.

AUTHOR INFORMATION

Corresponding Author

Amrit Puzari − *National Institute of Technology Nagaland, Dimapur 797103, Nagaland, India;* orcid.org/0000-0001-9485-6237; Email: amrit09us@yahoo.com

Authors

Dhiraj Dutta − *National Institute of Technology Nagaland, Dimapur 797103, Nagaland, India*

Rama Dubey − *Defence Research Laboratory, Tezpur 784001, Assam, India*

Jyoti Prasad Borah − *National Institute of Technology Nagaland, Dimapur 797103, Nagaland, India;* orcid.org/0000-0003-0086-7926

Complete contact information is available at: https://pubs.acs.org/10.1021/acsomega.1c00083

Author Contributions

All authors contributed equally to the work.

Funding

No funding is accessed by the author from any external agency.

Notes

The authors declare no competing financial interest.

In this research work, there is no work requiring the ethical permission.

Consent of participation and publish was taken individually from all authors.

Additional data and materials are readily available if required.

■ ACKNOWLEDGMENTS

The authors thank the Director of DMSRDE, Kanpur, the Director of NIT Nagaland, the VC of Tezpur University, and the Director of DRL, Tezpur, for support in characterization using sophisticated instruments.

■ REFERENCES

(1) Liu, J.; Yang, H.; Gosling, S. N.; Kummu, M.; Flörke, M.; Pfister, S.; Hanasaki, N.; Wada, Y.; Zhang, X.; Zheng, C.; Alcamo, J.; Oki, T. Water Scarcity Assessments in the Past, Present, and Future. *Earth's Future* **2017**, 545−559.

(2) Alcamo, J.; Döll, P.; Henrichs, T.; Kaspar, F.; Lehner, B.; Rösch, T.; Siebert, S. Global Estimates of Water Withdrawals and Availability under Current and Future "Business-as-Usual" Conditions. *Hydrol. Sci. J.* **2003**, *48*, 339−348.

(3) Alcamo, J.; Henrichs, T. Critical Regions: A Model-Based Estimation of World Water Resources Sensitive to Global Changes. *Aquat. Sci.* **2002**, *64*, 352−362.

(4) Allman, A.; Daoutidis, P.; Arnold, W. A.; Cussler, E. L. Efficient Water Pollution Abatement. *Ind. Eng. Chem. Res.* **2019**, *58*, 22483−22487.

(5) Seckler, D.; Barker, R.; Amarasinghe, U. Water Scarcity in the Twenty-First Century. *Int. J. Water Resour. Dev.* **1999**, *15*, 29−42.

(6) Igwe, P. U.; Chukwudi, C. C.; Ifenatuorah, F. C.; Fagbeja, I. F.; Okeke, C. A. A Review of Environmental Effects of Surface Water Pollution. *Int. J. Adv. Eng. Res. Sci.* **2017**, *4*, 128−137.

(7) Kostecki, D. F. Water Pollution Control. *EOS, Trans. Am. Geophys. Union* **1970**, *51*, 862.

(8) Hennebique, A.; Boisset, S.; Maurin, M. Tularemia as a Waterborne Disease: A Review. *Emerging Microbes Infect.* **2019**, 1027−1042.

(9) Mandal, B. K.; Suzuki, K. T. Arsenic Round the World: A Review. *Talanta* **2002**, 201−235.

(10) Zhang, L.; Fang, M. Nanomaterials in Pollution Trace Detection and Environmental Improvement. *Nano Today* **2010**, *5*, 128−142.

(11) Neumann, N. F.; Smith, D. W.; Belosevic, M. Waterborne Disease: An Old Foe Re-Emerging. *J. Environ. Eng. Sci.* **2005**, *4*, 155−171.

(12) Kalhor, K.; Ghasemizadeh, R.; Rajic, L.; Alshawabkeh, A. Assessment of Groundwater Quality and Remediation in Karst Aquifers: A Review. *Groundwater Sustainable Dev.* **2019**, *8*, 104−121.

(13) Subba Rao, N. Iron Content in Groundwaters of Visakhapatnam Environs, Andhra Pradesh, India. *Environ. Monit. Assess.* **2008**, *136*, 437−447.

(14) Samantara, M. K.; Padhi, R. K.; Sowmya, M.; Kumaran, P.; Satpathy, K. K. Heavy Metal Contamination, Major Ion Chemistry and Appraisal of the Groundwater Status in Coastal Aquifer, Kalpakkam, Tamil Nadu, India. *Groundwater Sustainable Dev.* **2017**, *5*, 49−58.

(15) Tay, C. K.; Hayford, E. Levels, Source Determination and Health Implications of Trace Metals in Groundwater within the Lower Pra Basin, Ghana. *Environ. Earth Sci.* **2016**, *75*, 1236.

(16) Schwarzenbach, R. P.; Egli, T.; Hofstetter, T. B.; von Gunten, U.; Wehrli, B. Global Water Pollution and Human Health. *Annu. Rev. Environ. Resour.* **2010**, *35*, 109−136.

(17) Khan, F.; Wahab, R.; Rashid, M.; Khan, A.; Khatoon, A.; Musarrat, J.; Al-Khedhairy, A. A. The Use of Carbonaceous Nanomembrane Filter for Organic Waste Removal. In *Application of Nanotechnology in Water Research*; Scrivener Publishing LLC: 2014, pp. 115−152, DOI: 10.1002/9781118939314.ch6.

(18) Lantagne, D. S.; Clasen, T. F. Use of Household Water Treatment and Safe Storage Methods in Acute Emergency Response: Case Study Results from Nepal, Indonesia, Kenya, and Haiti. *Environ. Sci. Technol.* **2012**, *46*, 11352−11360.

(19) Petrusevski, B.; Sharma, S. K.; Kruis, F.; Omeruglu, P.; Schippers, J. C. Family Filter with Iron-Coated Sand: Solution for Arsenic Removal in Rural Areas. *Water Sci. Technol.: Water Supply* **2002**, *2*, 127−133.

(20) Kallman, E. N.; Oyanedel-Craver, V. A.; Smith, J. A. Ceramic Filters Impregnated with Silver Nanoparticles for Point-of-Use Water Treatment in Rural Guatemala. *J. Environ. Eng.* **2011**, *137*, 407−415.

(21) Hao, L.; Liu, M.; Wang, N.; Li, G. A Critical Review on Arsenic Removal from Water Using Iron-Based Adsorbents. *RSC Adv.* **2018**, *8*, 39545−39560.

(22) WHO. Guidelines for drinking water quality, pH in Drinking Water. WHO/SDE/WHO/03.04/12; WHO: 1996, *2 (1)*, 7.

(23) Marambio-Jones, C.; Hoek, E. M. V. A Review of the Antibacterial Effects of Silver Nanomaterials and Potential Implications for Human Health and the Environment. *J. Nanopart. Res.* **2010**, *12*, 1531−1551.

(24) Ma, M.-D.; Wu, H.; Deng, Z.-Y.; Zhao, X. Arsenic Removal from Water by Nanometer Iron Oxide Coated Single-Wall Carbon Nanotubes. *J. Mol. Liq.* **2018**, *259*, 369−375.

(25) Amini, M.; Abbaspour, K. C.; Berg, M.; Winkel, L.; Hug, S. J.; Hoehn, E.; Yang, H.; Johnson, C. A. Statistical Modeling of Global Geogenic Arsenic Contamination in Groundwater. *Environ. Sci. Technol.* **2008**, *42*, 3669−3675.

(26) Appelo, C. A. J.; de Vet, W. W. J. M. Modeling in Situ Iron Removal from Groundwater with Trace Elements Such as As. In *Arsenic in Ground Water*; Springer US: 2003,381−401, DOI: 10.1007/0-306-47956-7_14.

(27) Galaburri, G.; Peralta Ramos, M. L.; Lázaro-Martínez, J. M.; Fernández de Luis, R.; Arriortua, M. I.; Villanueva, M. E.; Copello, G. J. PH and Ion-Selective Swelling Behaviour of Keratin and Keratose 3D Hydrogels. *Eur. Polym. J.* **2019**, *118*, 1−9.

(28) Weidman, J.; Holsworth, R. E., Jr.; Brossman, B.; Cho, D. J.; St.Cyr, J.; Fridman, G. Effect of Electrolyzed High-PH Alkaline Water on Blood Viscosity in Healthy Adults. *J. Int. Soc. Sports Nutr.* **2016**, *13*, 45.

(29) Makvandi, P.; Iftekhar, S.; Pizzetti, F.; Zarepour, A.; Zare, E. N.; Ashrafizadeh, M.; Agarwal, T.; Padil, V. V. T.; Mohammadinejad, R.; Sillanpaa, M.; Maiti, T. K.; Perale, G.; Zarrabi, A.; Rossi, F. Functionalization of Polymers and Nanomaterials for Water Treatment, Food Packaging, Textile and Biomedical Applications: A Review. *Environ. Chem. Lett.* **2021**, *19*, 583−611.

(30) Manyangadze, M.; Chikuruwo, N. H. M.; Narsaiah, T. B.; Chakra, C. S.; Radhakumari, M.; Danha, G. Enhancing Adsorption Capacity of Nano-Adsorbents via Surface Modification: A Review. *S. Afr. J. Chem. Eng.* **2020**, 25−32.

(31) Barroso, G.; Li, Q.; Bordia, R. K.; Motz, G. Polymeric and Ceramic Silicon-Based Coatings-a Review. *J. Mater. Chem. A* **2019**, 1936−1963.

(32) Wang, X.; Feng, J.; Bai, Y.; Zhang, Q.; Yin, Y. Synthesis, Properties, and Applications of Hollow Micro-/Nanostructures. *Chem. Rev.* **2016**, 10983−11060.

(33) Jin, C.; Teng, G.; Gu, Y.; Cheng, H.; Fu, S. P.; Zhang, C.; Ma, W. Functionalized Hollow $MnFe_2O_4$ Nanospheres: Design, Applications and Mechanism for Efficient Adsorption of Heavy Metal Ions. *New J. Chem.* **2019**, *43*, 5879−5889.

(34) Wang, C.; Yan, J.; Cui, X.; Cong, D.; Wang, H. Preparation and Characterization of Magnetic Hollow PMMA Nanospheres via in Situ Emulsion Polymerization. *Colloids Surf., A* **2010**, *363*, 71−77.

(35) Ahangaran, F.; Navarchian, A. H.; Picchioni, F. Material Encapsulation in Poly(Methyl Methacrylate) Shell: A Review. *J. Appl. Polym. Sci.* **2019**, *136*, 48039.

(36) Salabat, A.; Mirhoseini, F.; Valirasti, R. Engineering Poly(Methyl Methacrylate)/Fe_2O_3 Hollow Nanospheres Composite Prepared in Microemulsion System As a Recyclable Adsorbent for Removal of Benzothiophene. *Ind. Eng. Chem. Res.* **2019**, *58*, 17850−17858.

(37) Dubey, R.; Bag, D. S.; Varadan, V. K.; Lal, D.; Mathur, G. N. Polyaniline Coating on Glass and PMMA Microspheres. *React. Funct. Polym.* **2006**, *66*, 441−445.

https://doi.org/10.1021/acsomega.1c00083
ACS Omega 2021, 6, 10095−10105

(38) Kausar, A. Polymer Coating Technology for High Performance Applications: Fundamentals and Advances. *J. Macromol. Sci., Part A* **2018**, 440−448.
(39) Fotovvati, B.; Namdari, N.; Dehghanghadikolaei, A. On Coating Techniques for Surface Protection: A Review. *J. Manuf. Mater. Process.* **2019**, *3*, 28.
(40) Juneja, R.; Roy, I. Surface Modified PMMA Nanoparticles with Tunable Drug Release and Cellular Uptake. *RSC Adv.* **2014**, *4*, 44472−44479.
(41) Elvira, C.; Fanovich, A.; Fernández, M.; Fraile, J.; San Román, J.; Domingo, C. Evaluation of Drug Delivery Characteristics of Microspheres of PMMA-PCL-Cholesterol Obtained by Supercritical-CO_2 Impregnation and by Dissolution-Evaporation Techniques. *J. Controlled Release* **2004**, *99*, 231−240.
(42) Nie, L.; Zeng, X.; Guo, H.; Zhang, L. Poly(N-Isopropylacrylamide)-Coated Thermoresponsive/Magnetic/Fluorescent Multifunctional Microspheres. *Adv. Sci. Lett.* **2012**, *10*, 202−207.
(43) Dong, Y. Z.; Han, W. J.; Choi, H. J. Polyaniline Coated Core-Shell Typed Stimuli-Responsive Microspheres and Their Electrorheology. *Polymers* **2018**, *10*, 299.
(44) Philippova, O.; Barabanova, A.; Molchanov, V.; Khokhlov, A. Magnetic Polymer Beads: Recent Trends and Developments in Synthetic Design and Applications. *Eur. Polym. J.* **2011**, *47*, 542−559.
(45) Li, G.; Liu, G.; Kang, E. T.; Neoh, K. G.; Yang, X. PH-Responsive Hollow Polymeric Microspheres and Concentric Hollow Silica Microspheres from Silica-Polymer Core-Shell Microspheres. *Langmuir* **2008**, *24*, 9050−9055.
(46) Tan, Z.; Wang, S.; Hu, Z.; Chen, W.; Qu, Z.; Xu, C.; Zhang, Q.; Wu, K.; Shi, J.; Lu, M. PH-Responsive Self-Healing Anticorrosion Coating Based on a Lignin Microsphere Encapsulating Inhibitor. *Ind. Eng. Chem. Res.* **2020**, *59*, 2657−2666.
(47) Bhadra, J.; Alkareem, A.; Al-Thani, N. A Review of Advances in the Preparation and Application of Polyaniline Based Thermoset Blends and Composites. *J. Polym. Res.* **2020**, *27*, 122.
(48) Li, Y.; Wang, B.; Feng, W. Chiral Polyaniline with Flaky, Spherical and Urchin-like Morphologies Synthesized in the l-Phenylalanine Saturated Solutions. *Synth. Met.* **2009**, *159*, 1597−1602.
(49) Nagarajan, R.; Liu, W.; Kumar, J.; Tripathy, S. K.; Bruno, F. F.; Samuelson, L. A. Manipulating DNA Conformation Using Intertwined Conducting Polymer Chains. *Macromolecules* **2001**, *34*, 3921−3927.
(50) Yuan, G.-L.; Kuramoto, N. Water-Processable Chiral Polyaniline Derivatives Doped and Intertwined with Dextran Sulfate: Synthesis and Chiroptical Properties. *Macromolecules* **2002**, *35*, 9773−9779.
(51) Xu, F.; Ma, L.; Gan, M.; Tang, J.; Li, Z.; Zheng, J.; Zhang, J.; Xie, S.; Yin, H.; Shen, X.; Hu, J.; Zhang, F. Preparation and Characterization of Chiral Polyaniline/Barium Hexaferrite Composite with Enhanced Microwave Absorbing Properties. *J. Alloys Compd.* **2014**, *593*, 24−29.
(52) Tian, X.; Meng, F.; Meng, F.; Chen, X.; Guo, Y.; Wang, Y.; Zhu, W.; Zhou, Z. Synergistic Enhancement of Microwave Absorption Using Hybridized Polyaniline@helical CNTs with Dual Chirality. *ACS Appl. Mater. Interfaces* **2017**, *9*, 15711−15718.
(53) Cheng, Z.; Zhang, D.; Luo, X.; Lai, H.; Liu, Y.; Jiang, L. Superwetting Shape Memory Microstructure: Smart Wetting Control and Practical Application. *Adv. Mater.* **2021**, *33*, 2001718.
(54) Guo, F.; Guo, Z. Inspired Smart Materials with External Stimuli Responsive Wettability: A Review. *RSC Adv.* **2016**, 36623−36641.
(55) Rehman, A.; Houshyar, S.; Reineck, P.; Padhye, R.; Wang, X. Multifunctional Smart Fabrics through Nanodiamond-Polyaniline Nanocomposites. *ACS Appl. Polym. Mater.* **2020**, *2*, 4848−4855.
(56) Kelly, F. M.; Meunier, L.; Cochrane, C.; Koncar, V. Polyaniline: Application as Solid State Electrochromic in a Flexible Textile Display. *Displays* **2013**, *34*, 1−7.
(57) Abd Razak, S. I.; Wahab, I. F.; Fadil, F.; Dahli, F. N.; Md Khudzari, A. Z.; Adeli, H. A Review of Electrospun Conductive Polyaniline Based Nanofiber Composites and Blends: Processing Features, Applications, and Future Directions. *Adv. Mater. Sci. Eng.* **2015**, 1.
(58) Dubey, R.; Dutta, D.; Shami, T. C.; Bhasker Rao, K. U. Preparation and Chiro-Optical Characterization of Polyaniline Doped with (+) or (−)-2-Pyrrolidone-5-Carboxylic Acid (PCA). *Chirality* **2011**, *23*, 320−325.
(59) Sapurina, I. Y.; Shishov, M. A. Oxidative Polymerization of Aniline: Molecular Synthesis of Polyaniline and the Formation of Supramolecular Structures. In *New Polymers for Special Applications*; InTech: 2012, DOI: 10.5772/48758.
(60) Parida, P.; Mishra, S. C.; Sahoo, S.; Behera, A.; Nayak, B. P. Development and Characterization of Ethylcellulose Based Microsphere for Sustained Release of Nifedipine. *J. Pharm. Anal.* **2016**, *6*, 341−344.
(61) Ibrahim, K. A. Synthesis and Characterization of Polyaniline and Poly(Aniline-Co-o-Nitroaniline) Using Vibrational Spectroscopy. *Arabian J. Chem.* **2017**, *10*, S2668−S2674.
(62) Trchová, M.; Stejskal, J. Polyaniline: The Infrared Spectroscopy of Conducting Polymer Nanotubes (IUPAC Technical Report). *Pure Appl. Chem.* **2011**, *83*, 1803−1817.
(63) Ajeel, K. I.; Kareem, Q. S. Synthesis and Characteristics of Polyaniline (PANI) Filled by Graphene (PANI/GR) Nano-Films. *J. Phys.: Conf. Ser.* **2019**, *1234*, No. 012020.
(64) Kohut-Svelko, N.; Reynaud, S.; François, J. Synthesis and Characterization of Polyaniline Prepared in the Presence of Nonionic Surfactants in an Aqueous Dispersion. *Synth. Met.* **2005**, *150*, 107−114.
(65) Mishima, S.; Iikura, H.; Ougizawa, T. Study of Adhesion between Microspheres and Rubber Surfaces Accompanied by Meniscus Formation and Sedimentation. *Appl. Adhes. Sci.* **2017**, *5*, 5.
(66) Gulrez, S. K. H.; Ali Mohsin, M. E.; Shaikh, H.; Anis, A.; Pulose, A. M.; Yadav, M. K.; Qua, E. H. P.; Al-Zahrani, S. M. A Review on Electrically Conductive Polypropylene and Polyethylene. *Polym. Compos.* **2014**, 900−914.
(67) De Albuquerque, J. E.; Mattoso, L. H. C.; Faria, R. M.; Masters, J. G.; MacDiarmid, A. G. Study of the Interconversion of Polyaniline Oxidation States by Optical Absorption Spectroscopy. *Synth. Met.* **2004**, *146*, 1−10.
(68) Wudl, F.; Angus, R. O., Jr.; Lu, F. L.; Allemand, P. M.; Vachon, D.; Nowak, M.; Liu, Z. X.; Schaffer, H.; Heeger, A. J. Poly-p-Phenyleneamineimine: Synthesis and Comparison to Polyaniline. *J. Am. Chem. Soc.* **1987**, *109*, 3677−3684.
(69) Ali Mohsin, M. E.; Shrivastava, N. K.; Arsad, A.; Basar, N.; Hassan, A. The Effect of PH on the Preparation of Electrically Conductive and Physically Stable PANI/Sago Blend Film via in Situ Polymerization. *Front. Mater.* **2020**, *7*, 20.
(70) Huang, W. S.; MacDiarmid, A. G. Optical Properties of Polyaniline. *Polymer* **1993**, *34*, 1833−1845.
(71) Shacklette, L. W. Dipole and Hydrogen-Bonding Interactions in Polyaniline: A Mechanism for Conductivity Enhancement. *Synth. Met.* **1994**, *65*, 123−130.
(72) De Medeiros, D. W.; Dos Santos, D. S.; Dantas, T. N.; Pereira, M. R.; Giacometti, A.; Fonseca, J. L. Zeta Potential and Doping in Polyaniline Dispersions. *Mater. Sci.* **2003**, *21*, 251−257.

https://doi.org/10.1021/acsomega.1c00083
ACS Omega 2021, 6, 10095−10105